

Article

Structure and Properties of Ti-Al-Ta and Ti-Al-Cr Cladding Layers Fabricated on Titanium

Daria V. Lazurenko ^{1,*}, Mikhail G. Golkovsky ², Andreas Stark ³ , Florian Pyczak ³, Ivan A. Bataev ¹ , Alexey A. Ruktuev ¹, Ivan Yu. Petrov ¹ and Ilia S. Laptev ¹

¹ Research Laboratory of Physical and Chemical Technologies and Functional Materials, Materials Science Department, Novosibirsk State Technical University, Karl Marks Str. 20, 630073 Novosibirsk, Russia; ivanbataev@ngs.ru (I.A.B.); alex47@211.ru (A.A.R.); petrov.2017@stud.nstu.ru (I.Y.P.); ilya_laptev_nstu@mail.ru (I.S.L.)

² Laboratory of Industrial Accelerators, Budker Institute of Nuclear Physics of Siberian Branch, Russian Academy of Sciences, Lavrentiev Avenue 11, 630090 Novosibirsk, Russia; golkovski@mail.ru

³ Helmholtz Zentrum Hereon, Institute of Materials Physics, Max-Planck-Straße 1, 21502 Geesthacht, Germany; andreas.stark@hereon.de (A.S.); florian.pyczak@hereon.de (F.P.)

* Correspondence: pavlyukova_87@mail.ru

Abstract: Being one of the most high-demand structural materials, titanium has several disadvantages, including low resistance to high-temperature oxidation and wear. The properties of titanium and its alloys can be improved by applying protective intermetallic coatings. In this study, 2 mm thick Ti-Al-Ta and Ti-Al-Cr layers were obtained on titanium workpieces by a non-vacuum electron-beam cladding. The microstructure and phase compositions of the samples were different for various alloying elements. The Cr-containing layer consisted of α_2 , γ , and B2 phases, while the Ta-containing layer additionally consisted of ω' phase ($P\bar{3}m1$). At the same atomic concentrations of aluminum and an alloying element in both layers, the volume fraction of the B2/ ω phase in the Ti-41Al-7Ta alloy was significantly lower than in the Ti-41Al-7Cr alloy, and the amount of γ phase was higher. The Ti-41Al-7Cr layer had the highest wear resistance (2.1 times higher than that of titanium). The maximum oxidation resistance (8 times higher compared to titanium) was observed for the Ti-41Al-7Ta layer.

Keywords: non-vacuum electron beam cladding; titanium aluminides; ω -phase; oxidation; wear



Citation: Lazurenko, D.V.; Golkovsky, M.G.; Stark, A.; Pyczak, F.; Bataev, I.A.; Ruktuev, A.A.; Petrov, I.Y.; Laptev, I.S. Structure and Properties of Ti-Al-Ta and Ti-Al-Cr Cladding Layers Fabricated on Titanium. *Metals* **2021**, *11*, 1139. <https://doi.org/10.3390/met11071139>

Academic Editors: Maciej Motyka, Thomas Niendorf and Frank Czerwinski

Received: 22 June 2021
Accepted: 16 July 2021
Published: 19 July 2021

Publisher's Note: MDPI stays neutral with regard to jurisdictional claims in published maps and institutional affiliations.



Copyright: © 2021 by the authors. Licensee MDPI, Basel, Switzerland. This article is an open access article distributed under the terms and conditions of the Creative Commons Attribution (CC BY) license (<https://creativecommons.org/licenses/by/4.0/>).

1. Introduction

Titanium and Ti-based alloys are widely used in aerospace engineering, shipbuilding, chemical engineering, and power engineering due to their outstanding properties, such as high strength, excellent corrosion resistance, and low density. However, at elevated temperatures and under friction conditions, the application of titanium is limited. Titanium is characterized by a high reactivity with oxygen when heated. Long exposure of titanium to air at a temperature above 700–800 °C results in forming an oxide scale that can be easily peeled off from the surface [1,2]. Furthermore, the oxygen absorbed by titanium is spent not only on the formation of a scale but also dissolves in it [3,4]. Finally, these factors have a negative impact on the durability of parts being used at high temperatures. The low wear resistance of titanium is explained by its high tendency to adhesion during friction. Its thin natural oxide film is easily destroyed by friction, and pure titanium starts to interact with the counter body. Furthermore, due to the low thermal conductivity of Ti, its high susceptibility to work hardening, which causes a local increase in strength in plastically deformed areas, and also due to enrichment with atmospheric gases, which provides additional strength to contact regions [5], destruction of adhesive bonds during friction occurs in the depths of the metal, which leads to the formation of so-called tear-outs and deep-laid damages. Thus, although titanium can be used in various friction units (fasteners, threaded joints, radial thrust roller bearings, rotating shafts, etc.), its utilization is impossible without preliminary surface treatment.

These problems can be solved by the formation of titanium aluminides on the surfaces of titanium workpieces. Having higher hardness and oxidation resistance as compared to titanium, titanium aluminides exhibit superior wear and high-temperature properties than titanium, which was proven in a number of studies [6–15]. However, when choosing the exact composition of the titanium aluminides suitable as wear coatings of titanium, it is necessary to find a compromise between the positive effects of titanium aluminides on the properties of Ti and their disadvantages, such as being generally brittle intermetallics.

For example, for binary Ti-Al coatings, it was found that with an increase in the titanium content, their resistance to oxidation and wear decreased together with the number of defects in the cladding layers [16]. In the coatings with 60 at.% of aluminum, multiple cracks were formed at the cladding stage. The number of cracks significantly decreased with a decrease in the aluminum content to 30 at.%, and below, however, the wear resistance dramatically reduced as well. To solve these problems, the binary Ti-Al coating can be alloyed with other elements. For example, the addition of chromium improves the ductility of γ -TiAl-based alloys and such refractory elements as niobium, molybdenum, and tungsten increase the resistance to oxidation and creep [17,18]. Microalloying additives (Si, B, C), as a rule, further improve the creep resistance [17,19]. The third and fourth generations of γ -TiAl-based alloys with a high concentration of niobium or tantalum (4–8 at.%) are recently in the focus of attention due to a better balance of properties and improved workability [20–22]. However, as mentioned above, when titanium aluminides are applied as protective coatings on titanium, they can be especially prone to cracking due to stresses induced by the difference in physical properties of titanium and intermetallic alloys. In this case, the issue of plasticity becomes critical. It was mentioned in [23] that alloys based on γ -TiAl with a high chromium content could exhibit superplasticity even in the as-cast state. For this reason, an alloy with 4–8 at.% Cr can be considered as a rational choice for application on titanium as a protective layer.

In our previous study [24], we synthesized high-quality γ -TiAl-based surface layers with niobium additions on commercially pure titanium workpieces by non-vacuum electron-beam cladding. It was shown that cladding layers with 2–8 at.% Nb additions had improved oxidation and wear resistance compared to titanium. In this study, we synthesized γ -TiAl protective layers with Ta and Cr additions on the pure titanium surfaces to estimate the contribution of naturally different elements in the structure and phase formation of the alloys in these conditions and thoroughly analyze the structure-properties relationship.

2. Materials and Methods

Non-vacuum electron beam cladding was used as a method to fabricate protective intermetallic layers on pure titanium. The experiments were carried out using an ELV-6 electron beam accelerator developed by the Budker Institute of Nuclear Physics (Novosibirsk, Russia). A detailed description of this technology and equipment can be found elsewhere [16,24].

Commercially pure Ti (0.09 wt.% Fe, 0.02 wt.% Cr, 0.02 wt.% Ni, 0.01 wt.% V, 0.01 wt.% C) was used as a base material. The dimensions of the workpieces were $100 \times 50 \times 12 \text{ mm}^3$. The powders of Ti, Al, Ta, Cr, and a flux (LiF) were preliminarily mixed and evenly distributed on the pure titanium workpieces. The flux was needed to prevent the oxidation of the melt since the process was carried out in the air. The amount of powder mixture per square centimeter of the sample was equal to 0.45 g. The content of elements in the starting powder mixtures is given in Table 1. The intended compositions of the coatings had to correspond to the Ti-45Al-8Cr and Ti-45Al-8Ta alloys (at.%).

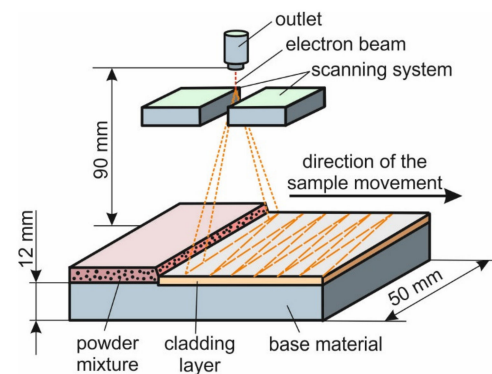
It should be noted that during the cladding, both powders and a surface layer of a workpiece are remelted. The preliminary experiments found that due to the mixing with titanium, the concentration of alloying elements in the cladding layer is approximately two times lower than that in the starting powder. For this reason, the starting mixtures either did not contain titanium or contained only a small amount of it (Table 1).

Table 1. Compositions of the powder mixtures, g.

Sample Designation	Ti	Al	Cr	Ta	LiF
Ti-41Al-7Cr	1.9	6.8	2.2	-	11.13
Ti-41Al-7Ta	-	4.4	-	7.33	10.6

The actual composition of the cladding layers slightly differed from the intended one due to the scattering of the powder mixture during electron-beam processing, which is especially common for such lightweight elements as aluminum. The actual average compositions (at. %) measured after the experiments are shown in Table 1 in the sample designation column. They will be used further in the text for the designation of the samples.

The treatment of workpieces with an electron beam injected into the air atmosphere was carried out with the following parameter sets. The electron energy and beam current were 1.4 MeV and 20 mA, respectively. The samples were moved under the electron beam at a speed of 10 mm/s. The distance from the outlet of the accelerator to the sample was 90 mm. The diameter of the electron beam on the sample was approximately 10 mm. The processing was carried out in scanning mode with a scan direction perpendicular to the direction of the sample movement with a frequency of 50 Hz and an amplitude of 25 mm. The electron beam power and the energy density for these conditions were 28 kW and 5.6 kJ/cm², respectively. The scheme of the process is shown in Figure 1.

**Figure 1.** Scheme of the electron beam treatment of a sample.

The specimens for material characterization were prepared according to the standard technique described in ASTM E3–11 (2017). The microstructure was investigated by scanning electron microscopy (SEM) using an LEO Gemini 1530 (Carl Zeiss AG, Oberkochen, Germany) microscope equipped with an Octane Plus (AMETEK EDAX, Mahwah, NJ, USA) energy dispersive X-ray (EDX) detector.

The phase composition of the materials was investigated by synchrotron X-ray diffraction (XRD). Diffraction patterns were obtained at Petra III synchrotron radiation source of the Deutsches Elektronen-Synchrotron (DESY, Hamburg, Germany) at the High Energy Materials Science Beamline (P07) operated by Helmholtz-Zentrum Hereon. The radiation energy was 100 keV, which corresponds to a wavelength of 0.124 Å. The spot size was 1 × 1 mm². The distance from the sample to the detector was 1837 mm. Diffraction rings were recorded using a Perkin Elmer XRD1621 (Perkin-Elmer Corp., Waltham, MA, USA) 2D detector with a resolution of 2048 × 2048 pixels and a pixel size of 200 × 200 μm² in the transmission mode. The diffraction rings were azimuthally integrated and plotted as intensity vs. 2θ. The phase composition was analyzed using the ICDD PDF-4 database. In addition, the lattice parameters and volume fractions of phases were calculated by the Rietveld analysis performed using the MAUD software [25].

The wear performance of the samples was estimated using a friction test against fixed abrasive particles according to GOST 17367-71 standard (the closest analog is the ASTM G132-96 standard). Specimens for testing with a diameter of 2 mm and a length of 12 mm were cut out from the samples in the direction perpendicular to the interface between the

base metal and the cladding layer. Corundum abrasive paper (P150) was used as a counter surface. The specimens were placed in a holder and pressed against a rotating disk with an abrasive paper with a constant force of 3 N. The test duration was 60 s; the disk rotation speed was 60 rpm. During the test, the specimens moved relative to the paper along the Archimedes spiral. Pure Ti was used as a reference sample. The relative wear resistance of the samples was calculated using the following equation:

$$\varepsilon = \frac{\Delta m_r}{\Delta m_t} \left(\frac{\rho_t}{\rho_r} \right) \quad (1)$$

where ρ_t , ρ_r are the densities of the sample and the reference material, respectively, and Δm_r , Δm_t are mass losses per 60 s test duration of the reference and the sample. The density of the samples was determined by hydrostatic weighing.

Surface topography after wear tests was studied using a Zygo NewView 7300 (Zygo Corporation, Middlefield, CT, USA) optical profiler.

Before oxidation tests, the cladding layers were cut out from the base material to exclude the influence of pure titanium on the results of the test. The dimensions of the specimens used for the experiments were $10 \times 20.5 \times 1.5 \text{ mm}^3$. The specimens were preliminarily ground using P1000 abrasive paper and then cleaned in acetone. The prepared pieces were placed in corundum crucibles and heated in a laboratory furnace at $800 \text{ }^\circ\text{C}$ in air. The total oxidation time was 200 h. The samples were removed from the furnace every 20 h, then cooled and weighed using an analytical balance with an accuracy of 10^{-4} g . Mass gain (Δm) was calculated as follows:

$$\Delta m = \frac{\Delta w}{s} \quad (2)$$

where Δw is a mass change after every testing cycle, and s is the specimen's area.

An ARL X'TRA (Thermo Fisher Scientific, Waltham, MA, USA) laboratory diffractometer was used to estimate the phase composition of an oxide scale after oxidation. Diffraction patterns were obtained using $\text{CuK}\alpha$ radiation with a step size of 0.05° and a dwell time of 5 s.

3. Results

3.1. Microstructure and Phase Compositions

The structure of the cladding layers was thoroughly characterized using a combination of XRD and SEM together with EDX.

3.1.1. Results of Synchrotron X-ray Diffraction Analysis

Analysis of the phase composition carried out using synchrotron X-ray diffraction revealed three different phases in the Ti-41Al-7Cr sample and four phases in the Ti-41Al-7Ta sample (Figure 2). A short description of these phases is summarized in Table 2.

Table 2. Crystal structure, formation routes, and selected properties of phases in Ti-Al-based alloys [17,26–28].

Phase	Space Group	Pearson Symbol	Composition, Homogeneity Range	Reactions	Young's Modulus (E), GPa	Yield Strength, MPa	Fracture Toughness (K1c), $\text{MPa}/\text{m}^{3/2}$
α_2 (Ti ₃ Al)	P6 ₃ /mmc	hP8	22–35 at.% Al	hcp → Ti ₃ Al (congruent)	100–145	700–990	13–42
γ (TiAl)	P4/mmm	tP4	35–48 at.% Al	L + hcp → AlTi (peritectic)	160–180	400–650	10–20
β /B2	Im $\bar{3}$ m/Pm $\bar{3}$ m	cI2/cP2	~39–48 at.% Al, ~47–63 at.% Ti, ~13–22 at.% X	L → bcc (congruent) → B2 (ordering) B2 → ω'	140	-	-
ω / ω'	P6/mmm/P $\bar{3}$ m1	hP3/-		(diffusionless) → ω (ordering)	-	-	-

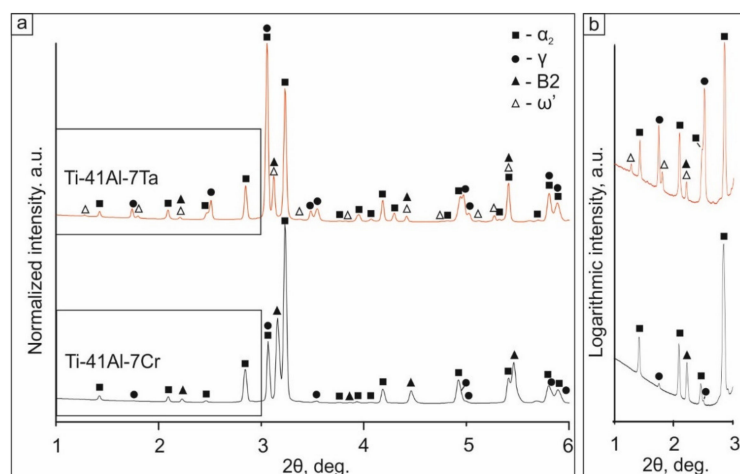


Figure 2. XRD patterns obtained from the samples (a). The same XRD patterns, but in the range from 1 to 3° plotted as logarithmic intensity over 2θ (b).

The XRD pattern of the Ti-41Al-7Cr sample contained reflections of α_2 , γ , and B2 phases. The intensity of α_2 and B2 peaks was much higher than that of γ . B2 is known as an ordered variant of the β -phase in alloys with a high concentration of refractory alloying elements (5–17 at.%). It is usually formed in TiAl-based alloys upon quenching [29,30]. The formation of B2 has been most frequently observed in Nb-containing alloys [17,31]. However, B2 in these alloys is often transformed into ω -type structures [29,30,32], which usually precipitate in the B2 matrix or at the B2/ γ grain boundaries [33].

Formation of the B2 phase in the Cr-containing TiAl-based alloys was previously observed in [34,35]. As noted in [36], the free energy of the B2 phase formation is lower than that of ω -related phases in the temperature range from 0 to 2000 K, which makes it possible to avoid the decomposition of B2 and the appearance of brittle ω -related phases in the structure of Cr-containing alloys. Our results are in good agreement with the literature data. Even under nonequilibrium conditions typical for electron-beam cladding, in particular high cooling rates [24], no precipitation of ω -related phases (including athermic ones) occurred.

The following volume fractions of different phases were found using Rietveld analysis: 71.7 vol.%, 26.5 vol.%, and 1.8 vol.% for α_2 , B2, and γ respectively (at $\sigma = 5.25$ and $R_w = 12.3$). The lattice parameter of the B2 phase was 3.179 Å. According to Jewett et al. [34], the B2 phase lattice parameter decreases with an increase in the chromium content, which is explained by a smaller atomic radius of chromium in comparison with aluminum and titanium. In our case, the lattice parameter of the B2 phase was similar but slightly lower than in the alloy TiCr_{0.5}Al_{0.5} obtained in [35] (18.2 at.% Al, 16.1 at.% Cr, 65.7 at.% Ti), which may indicate a deficiency of Al and enrichment with Cr. The lattice parameters of α_2 and γ were as follows: $a = 5.77$ Å, $c = 4.62$ Å and $a = 4.01$ Å, $c = 4.06$ Å, respectively.

In the Ti-42Al-7Ta cladding layer, in addition to the phases found in the Ti-42Al-7Cr sample, the ω' -phase was detected ($a = 4.55$ Å, $c = 5.54$ Å). This phase can be reliably distinguished from the ω phase by the peak at $2\theta = 1.27^\circ$ (Figure 2b). ω' is an intermediate phase that can form during B2 \rightarrow ω transition. B2 \rightarrow ω' transformation is a diffusionless process resulting in the conversion of the Pm $\bar{3}$ m lattice to a structure with the P $\bar{3}$ m1 symmetry [29]. The atomic positions in the ω' phase are the same as in B2. Thus, the ω' structure can be derived from B2 by lowering its symmetry. The ω' phase was detected in our previous study on Ti-Al-Nb cladding layers obtained by non-vacuum electron-beam treatment [24]. It is known from [37,38] that metastable ω -related phases can be formed during the fast cooling of alloys containing a high amount of β -stabilizers. The formation of cladding layers during electron-beam treatment occurs at high cooling rates of up to 10^4 °C/s [24], explaining diffusionless B2 \rightarrow ω' transition.

Despite the lack of information in the literature on the formation of the ω -related phases in ternary Ti-Al-Ta alloys (to the best of our knowledge, the ω phase in alloys with a composition similar to that discussed in our study was mentioned only in [39]), it can be expected that the effect of tantalum and niobium being both refractory β -stabilizing elements, is similar. At least, binary Ti-Ta alloys [40], and Ti-Ta alloys with minor additions of aluminum [41,42], are prone to form the ω phase. According to Rietveld analysis, the ω' volume fraction in the Ti-41Al-7Ta sample was low (about 1.1%). However, it is difficult to consider this value completely reliable since most of the ω phase peaks, except for those at small angles, coincide with B2 peaks ($a = 3.22 \text{ \AA}$). The volume fraction of the latter was estimated to be 3.7%. The α_2 and γ phases were predominant in the structure of the sample: 54.7 and 40.5 vol.%, respectively (at $R_w = 11.6$ and $\sigma = 1.64$). The lattice parameters of α_2 and γ phases ($a = 5.76 \text{ \AA}$, $c = 4.43 \text{ \AA}$ and $a = 4.01 \text{ \AA}$, $c = 4.08$, respectively) slightly differed from the parameters determined for the same phases in the Ti-42Al-7Cr alloy. This difference could arise from the partial dissolution of alloying elements characterized by different atomic radii in Ti_3Al and TiAl intermetallics, causing various distortions of their lattices.

3.1.2. Microstructure of the Samples

Microstructures of the cladding layers obtained on the pure titanium surfaces are shown in Figures 3 and 4. The results of EDX analysis of the local areas marked as Sp. in Figures 3 and 4 are given in Tables 3 and 4, respectively.

Table 3. Results of EDX analysis of different zones of the Ti-41Al-7Cr cladding layer labeled in Figure 3, at.%.

Spectrum (Sp.) No	Al	Ti	Cr
Spectrum 1	44.2	48.7	7.1
Spectrum 2	40.9	52.5	6.6
Spectrum 3	35.9	58.3	5.8

Table 4. Results of EDX analysis of different zones of the Ti-41Al-7Ta cladding layer labeled in Figure 4, at.%.

Spectrum (Sp.) No	Al	Ti	Ta
Spectrum 1	51.0	41.4	7.6
Spectrum 2	38.9	54.0	6.1
Spectrum 3	36.8	57.4	5.8
Spectrum 4	39.8	54.0	6.2
Spectrum 5	42.4	52.5	5.1
Spectrum 6	34.0	38.7	27.3

Micrographs of the samples obtained at low magnifications (Figures 3a and 4a) indicate the formation of high-quality defect-free layers. There were no signs of cracking in the coatings. The thickness of the cladding layers was 1–2 mm.

Due to the complex processes of melt flows, heat dissipation, absorption, and solidification, the distribution of elements in the direction from the surface (top part of Figures 3a and 4a) of the cladding layer to the base metal (bottom part of Figures 3a and 4a) was non-uniform (Figure 3a, Table 3). As a result, the content of aluminum and chromium gradually decreased, and titanium increased as it approached the pure titanium substrate. It indicates a more significant dilution of the cladding layer by titanium in the regions adjacent to the base material (2.7 times vs. 2 times in the top part of the cladding layer). In addition to the variation in the composition of the cladding layer along its depth, microstructural changes were also observed.

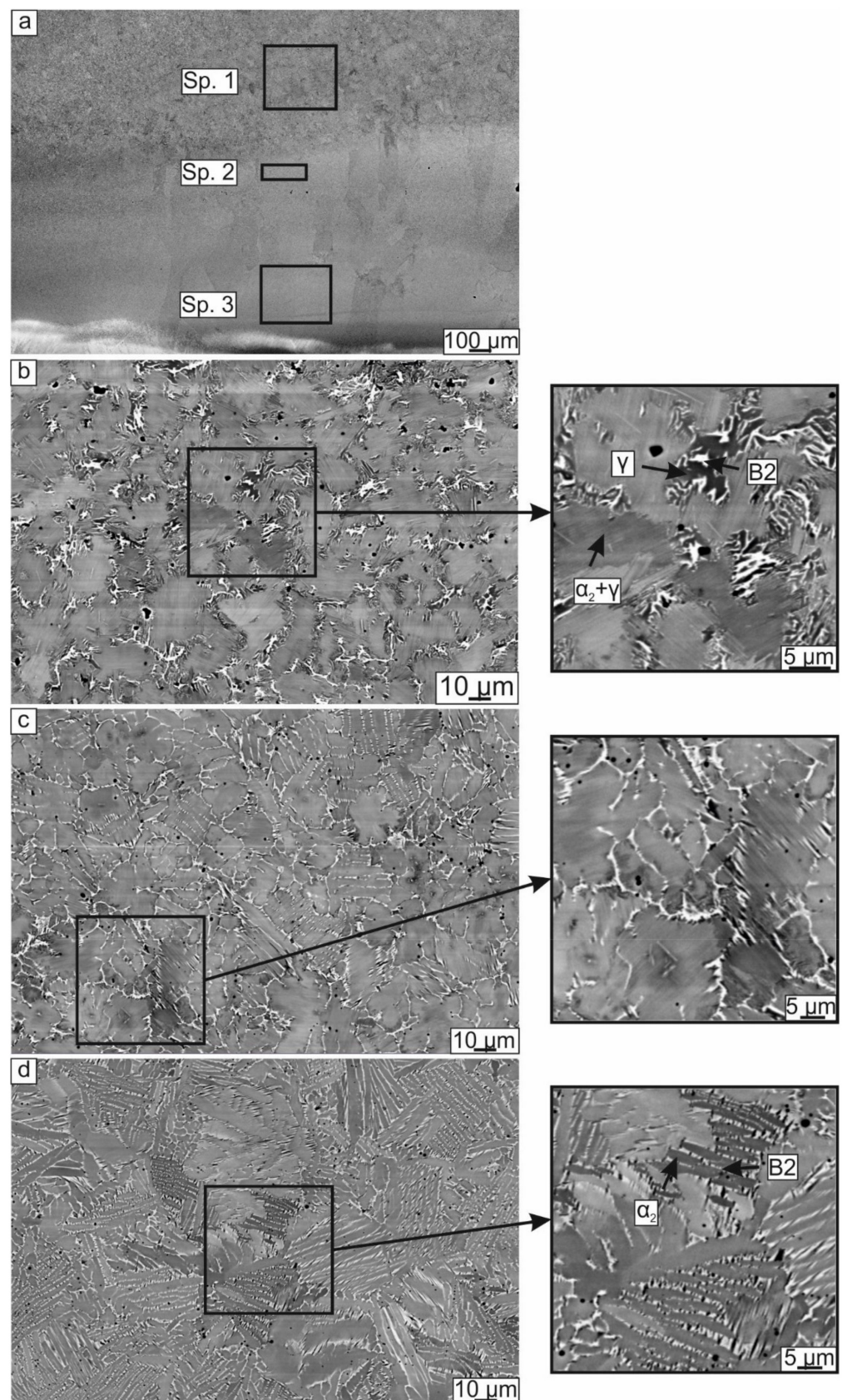


Figure 3. Microstructure of the Ti-41Al-7Cr cladding layer: (a) overview; (b–d) local areas of the cladding layer obtained in the direction from the surface of the cladding layer to the substrate. SEM images were obtained in backscattered electrons mode.

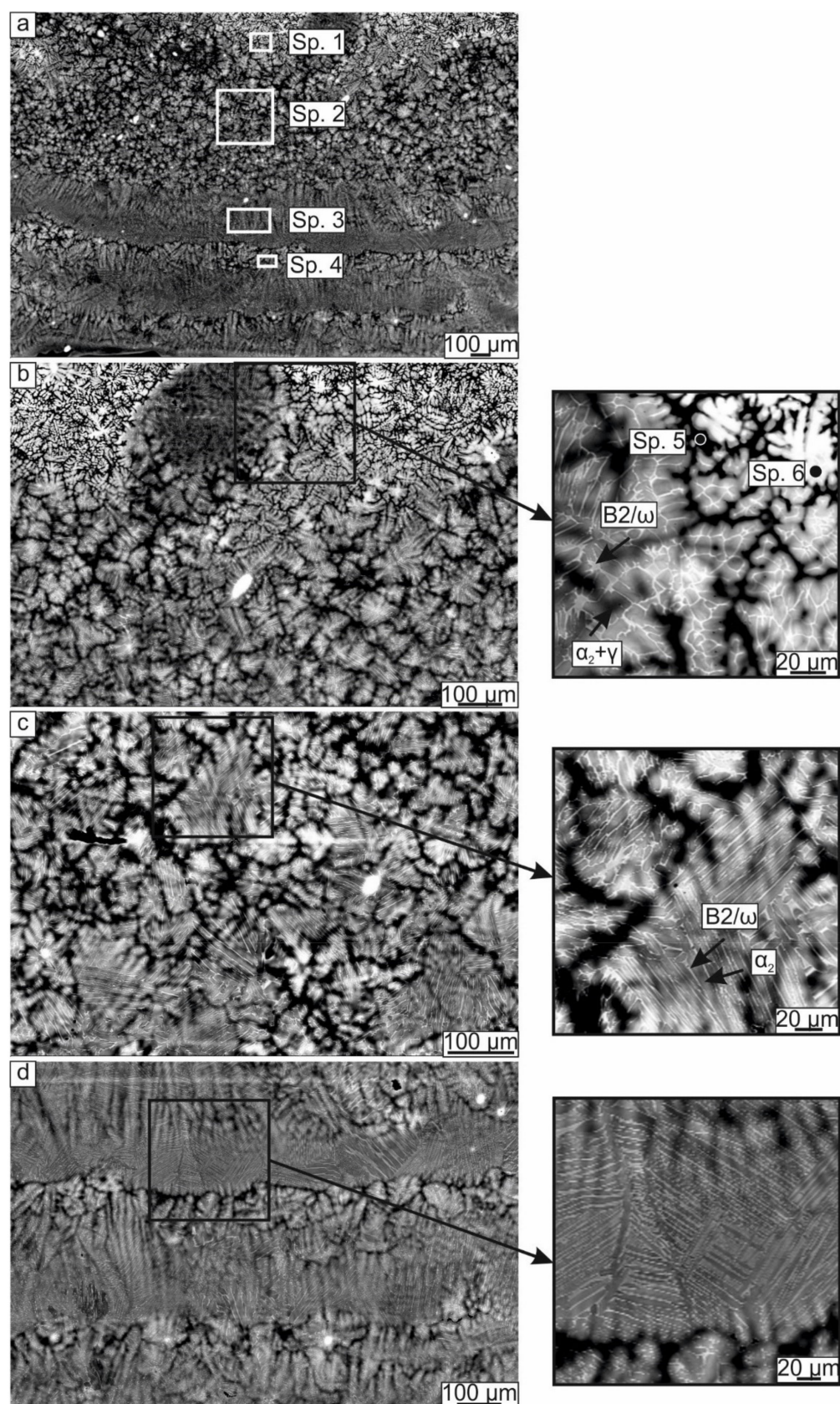


Figure 4. Microstructure of the Ti-41Al-7Ta cladding layer: (a) overview; (b–d) local areas of the cladding layer obtained in the direction from the surface of the cladding layer to the substrate. SEM images were obtained in backscattered electrons mode.

According to XRD analysis, three phases were formed in the Ti-41Al-7Cr sample, namely α_2 , γ , and B2. It is clearly seen at higher magnification (Figure 3b) that the microstructure of gray areas is lamellar. This type of structure usually corresponds to an $\alpha_2 + \gamma$ phase mixture. The lamellar regions are surrounded by a B2 + γ monovariant eutectic. Dark areas corresponded to the γ phase, while light zones to the B2 phase. Towards the titanium substrate, the structural components of the eutectic mixture were refined (Figure 3c,d), and the γ phase fraction decreased. In the vicinity of the substrate (Figure 3d), gray areas, which were characterized by a lamellar structure in Figure 3b were also refined and became elongated. In this zone, the lamellae in the microstructure of gray areas were not observed, suggesting that the phase composition of these areas changed from $\alpha_2 + \gamma$ to α_2 . Microstructural changes were in accordance with variations in the elemental composition of the cladding layer: with a decrease in the aluminum content in the direction from the surface to the substrate, the amount of γ phase decreased, and the fraction of α_2 increased.

The distribution of elements and phases in the cladding layer alloyed with tantalum was also uneven (Figure 4a, Table 4). The maximum percentage of aluminum was found in the top part of the cladding layer (51 at.%). In the lower part of the cladding material, a “layered” structure was formed (Figure 4a,d). The Ti/Al/Ta ratio slightly varied from layer to layer (Table 4, Spectra 3 and 4). The structure in different layers was also different. The upper part of the cladding layer enriched with aluminum had a pronounced dendritic structure (Figure 4b). The ratio of elements in the dendrites (Spectrum 6) and interdendritic regions (Spectrum 5) differed. The dendrites were characterized by a high tantalum content (up to 27 at.%), while interdendritic space was lean in tantalum and enriched with aluminum compared to the surrounding matrix. Such a distribution of elements is typical for as-cast alloys with a composition close to that considered in our study [43]. It is explained by the crystallization peculiarities of these alloys. Having a higher crystallization temperature, tantalum solidifies first, contributing to the formation of dendrite branches. Regions depleted in tantalum and enriched in low-melting aluminum form the interdendritic space.

A less inhomogeneous chemical distribution structure was formed below the zone described above, as evidenced by a less sharp contrast in the SEM image. The microstructure was represented by a mesh of the B2/ ω (light contrast in Figure 4b) and the $\alpha_2 + \gamma$ mixture (gray areas). Such a kind of structure can be formed upon rapid cooling of alloys with β -stabilizers (at a rate of 10 K/s) and was observed, for example, in materials obtained by directional solidification [44]. At fast cooling from the β -region, a part of the β -phase remains untransformed and retained in the final structure of the alloy, and the $\alpha_2 + \gamma$ lamellae are significantly refined and cannot be distinguished with SEM resolution.

It should be noted that a high concentration of aluminum was observed only in the near-surface zone of the cladding layer, which suggests that the γ -phase was mainly concentrated in the upper part of the coating. Figure 4c,d show the structures formed in the central and bottom parts of the cladding layer. These zones contained α_2 platelets and residual B2/ ω regions intertwined in the form of a fine basketweave microstructure. The layers labeled in Figure 4 as Spectrum 3 and 4, in addition to different ratios of elements, were characterized by different degrees of microstructure refinement (Figure 4c,d, respectively).

3.2. Properties of the Cladding Layers

To estimate the efficiency of Ti-41Al-7Ta and Ti-41Al-7Cr alloys as protective coatings for pure titanium, the wear resistance against fixed abrasive particles and oxidation resistance were tested since these properties are critical for titanium and its alloys.

3.2.1. Wear Behavior of the Cladding Layers with Respect to Titanium

Friction tests have shown that intermetallic layers with the addition of chromium and tantalum demonstrated the wear resistance 2.1 and 1.6 times higher, respectively, than that of pure titanium (Figure 5).

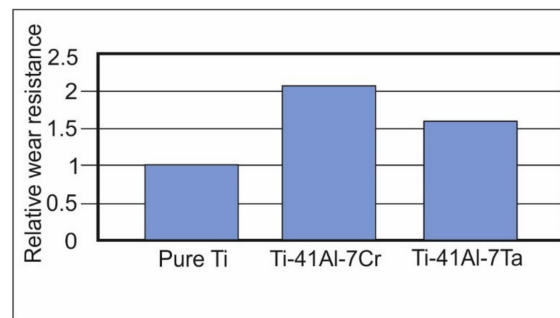


Figure 5. The relative wear resistance of the intermetallic layers obtained on pure titanium workpieces.

After the tests, analysis of the friction surfaces revealed a surface morphology that typically forms during abrasive wear. Grooves from the abrasive particles are clearly seen in Figure 6. The roughness of the surfaces of different samples after the tests slightly varied. The surface of the pure titanium was characterized by the maximum roughness ($R_a = 2.1 \mu\text{m}$). The cladding layers alloyed with chromium and tantalum had a roughness $R_a = 1.7$ and $R_a = 1.9 \mu\text{m}$, respectively. Thus, the surface of the Ti-41Al-7Ta intermetallic alloy after the wear test was rougher in comparison with the Cr-containing intermetallic layer.

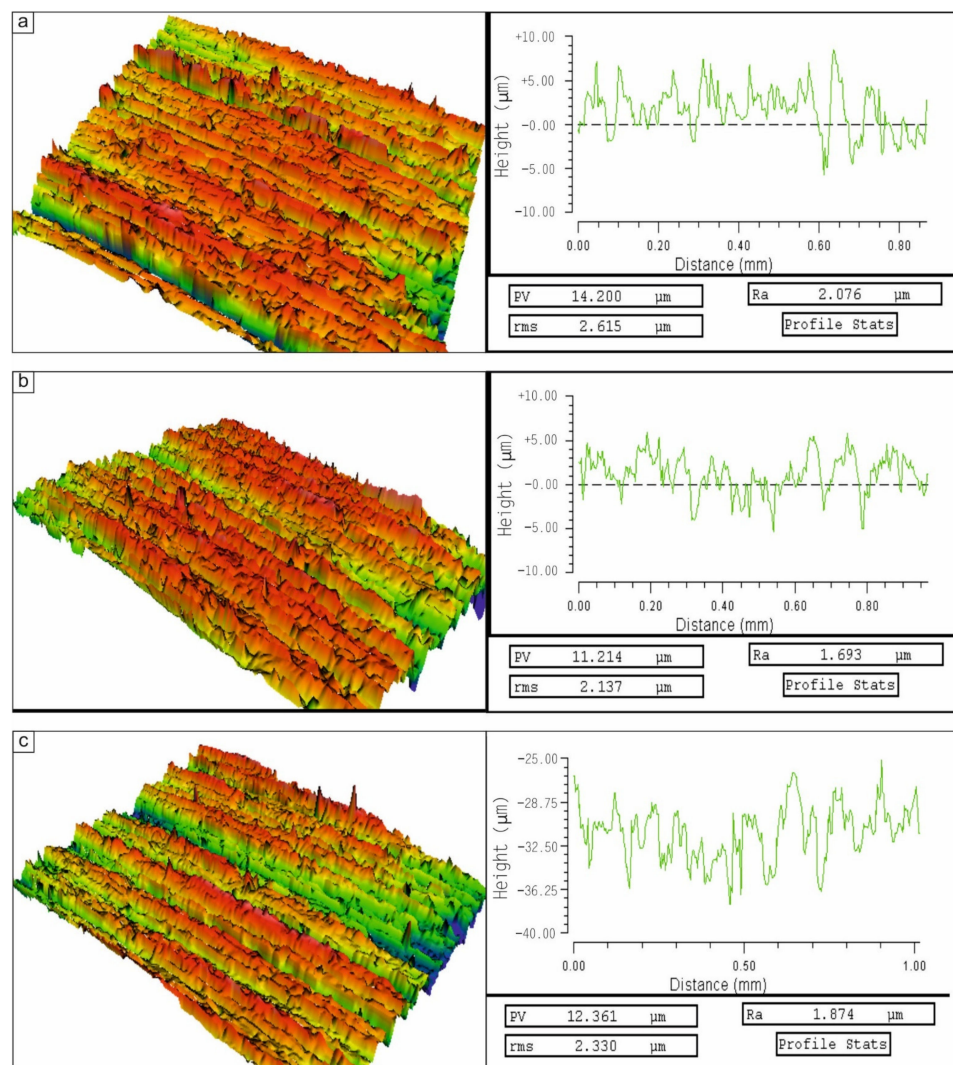


Figure 6. The surfaces of specimens after friction: pure titanium (a), Ti-41Al-7Cr cladding layer (b), Ti-41Al-7Ta cladding layer (c) after a friction test against fixed abrasive particles. Images and graphs were obtained using optical profilometry.

SEM study of the tested surfaces revealed numerous adhesive craters and deep plowing grooves (Figure 7). The appearance of tear-outs and trapping of abrasive particles on the surface indicated the seizure of pure titanium during friction (Figure 7a). For the intermetallic layer with compositions of Ti-41Al-7Cr and Ti-41Al-7Ta, the formation of tear-outs was not observed (Figure 7b,c, respectively). Apart from plowing grooves, traces of micro-cutting and micro-plowing were found on their surfaces. These phenomena are explained by the fact that although the hardness of the intermetallic alloy is higher than that of pure titanium, it is nevertheless much softer than hard abrasive particles. The cutting was accompanied by extrusion of material observed on the edges of the grooves (Figure 7c). It can be clearly seen on the worn surface of the Ti-41Al-7Ta sample. Apart from squeezing the material to the groove edges, the formation of wedges in front of the grooves can be observed. There were no signs of microfracture on the surfaces, that evidence some plasticity of intermetallic-based cladding layers.

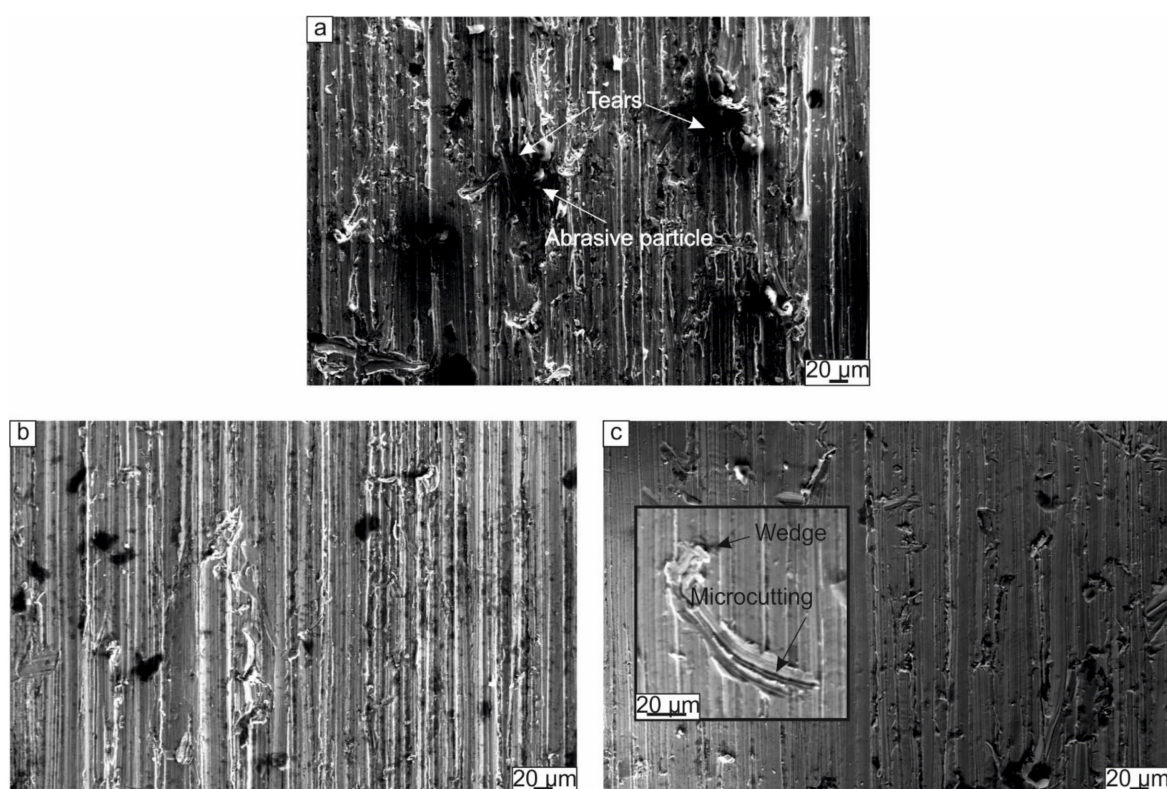


Figure 7. SEM images of the worn surfaces of pure titanium (a), Ti-41Al-7Cr cladding layer (b), Ti-41Al-7Ta cladding layer (c) after a friction test against fixed abrasive particles. SEM micrographs were obtained in the secondary electron mode.

It is known from the literature that the ω phase adversely affects the properties of TiAl-based alloys due to its high brittleness. However, there were no apparent signs of brittle fracture and chipping on the worn surface of the tantalum-containing alloy (Figure 7c). In addition, the fraction of the ω phase in the structure of these samples was extremely low, which suggests that its contribution to the wear properties was insignificant.

3.2.2. Oxidation Resistance of Cladding Materials

Results of oxidation resistance tests were plotted in Figure 8, which shows the mass gain (mass change after every testing cycle per unit area) vs. oxidation duration at 800 °C. The lowest mass gain was measured for Ti-41Al-7Ta alloy (less than 1 mg/cm²). It was almost 8-fold lower than that of pure Ti. The total mass gain of the Ti-41Al-7Cr cladding layer was 2.5 mg/cm².

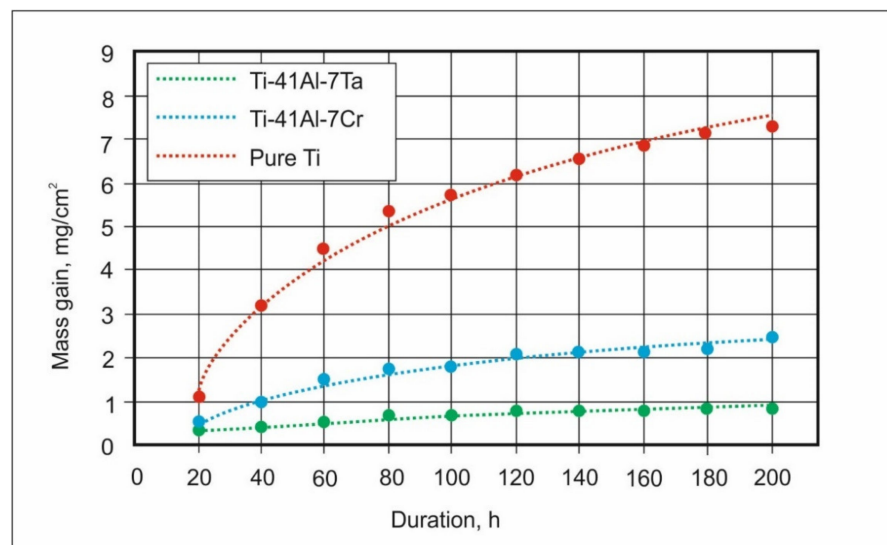


Figure 8. Mass gain during oxidation tests at 800 °C for 200 h.

It is clearly seen from the curves shown in Figure 8 that the rate of mass gains for all the samples is inversely related to time, i.e., as time increases, the rate of scale formation continuously decreases, which means that this process is controlled by diffusion. The shape of the curves gives information about the oxidation kinetics, which can be logarithmic, parabolic, or linear [45]. It is possible to determine the oxidation type using the equation characterizing the growth rate of the oxide layer:

$$\Delta m = k_p t^n \quad (3)$$

where Δm is a mass gain, k_p is the oxidation rate constant, n is the rate exponent, and t is the oxidation time.

The value of the exponent determines the curve growth character. If the n value is close to 0.5, then the oxidation kinetics has a parabolic character. From the plot of $\ln \Delta m$ vs. $\ln t$, the values of n for pure titanium, Ti-41Al-7Cr, and Ti-41Al-7Ta were found to be 0.77, 0.72, and 0.45, respectively. It means that only the sample Ti-71Al-7Ta completely follows the parabolic law. Mass gains vs. time plots for pure titanium and Ti-41Al-7Cr samples were better fitted by logarithmic curves, which means the faster oxidation at the first stages. Using the linear regression method, the growth rates of the oxide scale on the surfaces of the pure titanium, Ti-41Al-7Cr, and Ti-71Al-7Ta samples were found to be 0.03, 0.0096, and 0.0029 $\text{mg}\cdot\text{cm}^{-2}\cdot\text{h}^{-1}$, respectively. It means that the cladding layer with the tantalum addition is less prone to interaction with oxygen and the formation of an oxide scale on its surface.

The surfaces of the samples after the oxidation are shown in Figure 9. On the surface of the pure titanium specimen, a homogeneous oxide layer without obvious signs of delamination was formed (Figure 9a). The crystallites shown in Figure 9a were large and had a “blocky” morphology. It is known that at 800 °C, rutile forms on the surface of pure titanium since the concentration of other elements capable of reacting with oxygen in this alloy is extremely low [16].

In TiAl-based alloys, both titanium oxides and aluminum oxides can form [4]. However, a continuous alumina layer is required to ensure good oxidation resistance since the rapidly growing titanium oxide film does not provide adequate protection against reaction with oxygen. In binary and some ternary TiAl-based alloys, the formation of Al_2O_3 and TiO is thermodynamically favorable; however, TiO is rapidly oxidized to TiO_2 and, for this reason, is most often found in the oxidation products [17].

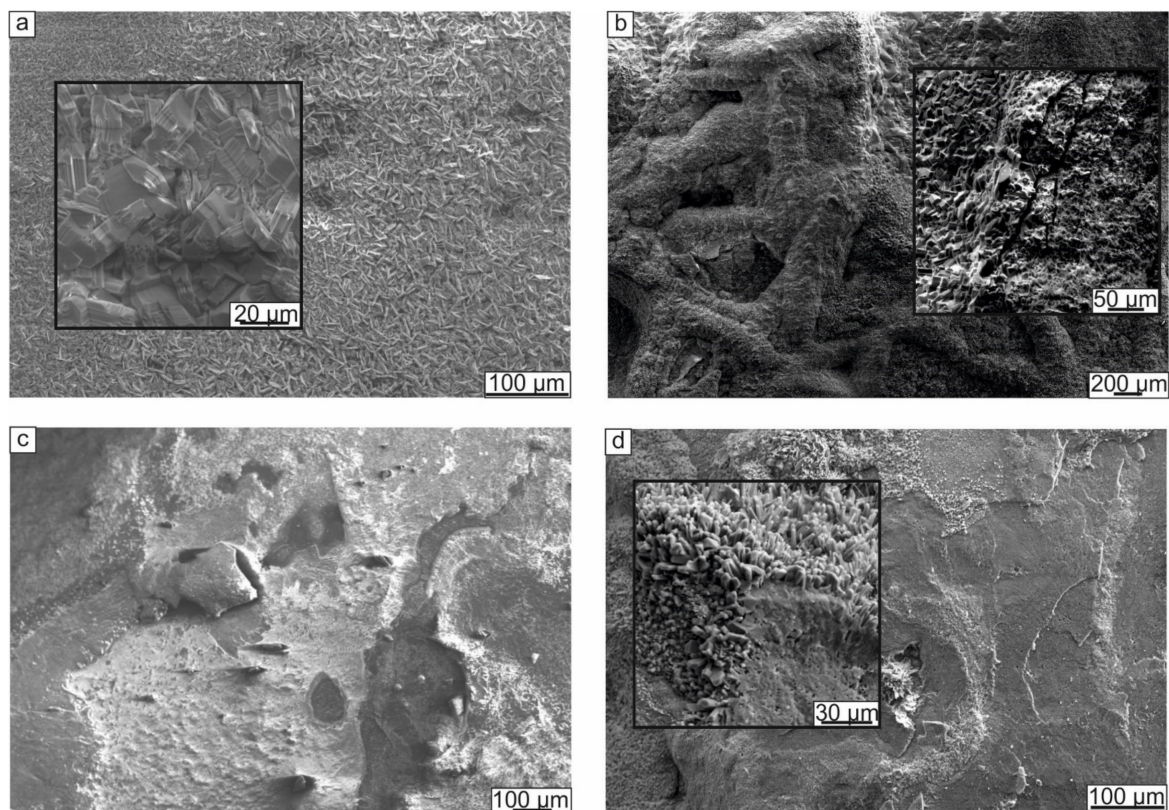


Figure 9. Oxide scales formed on the surfaces of samples after cyclic oxidation at 800 °C for 200 h: pure titanium (a), Ti-41Al-7Cr (b,c), Ti-41Al-7Ta (d). SEM micrographs were obtained in the secondary electron mode.

It is known that with an increase in the aluminum content in a binary alloy, its resistance to oxidation increases since the fraction of Al_2O_3 becomes higher. For this reason, Al_3Ti -based alloys exhibit the best oxidation resistance at high temperatures [46]. However, as mentioned above, the quality of the cladding layers significantly decreases with an increase in the aluminum content. The formation of Al-enriched brittle phases provokes cracks in the layer since the linear expansion coefficients of intermetallic compounds and the titanium differ significantly [16]. Additions of a third element to binary Ti-Al alloys with a moderate aluminum content can be a rational alternative to increasing the aluminum percentage in the alloy composition for achieving good oxidation resistance. In fact, the alloying element should promote the formation of a protective Al_2O_3 film and reduce the fraction of titanium oxides in the scale. Additionally, the fracture toughness of the alloy must remain at an acceptable level in order to avoid the formation of cracks in the cladding layers. From the perspective of plasticity increase, Cr as well as Mn and V, are beneficial, while Ta and other refractory elements increase the resistance to oxidation [17]. Thus, the results obtained in our study are quite expected.

At the same time, it was mentioned in a number of studies that Ti-Al-Cr-based intermetallic alloys with high chromium concentrations exhibited excellent properties at high-temperature exposure [47,48]. Being added to TiAl-based alloys, Cr changes the chemical activities of components favoring Al_2O_3 formation [47,49,50]. However, a positive effect of Cr mainly results from the Laves phase in such alloys, which has a low oxygen permeability and is capable of alumina scale formation despite relatively low Al content of 37–42 at.% in them [47].

In our study, the formation of $\text{Ti}(\text{Cr}, \text{Al})_2$ Laves phase has not been found. For this reason, a mixed oxide film consisting of Al_2O_3 and TiO_2 was formed on the Ti-41Al-7Cr sample surface after oxidation with a larger fraction of the latter oxide. This is confirmed by the significant difference in the intensity of the peaks from the two phases indicated above (Figure 10).

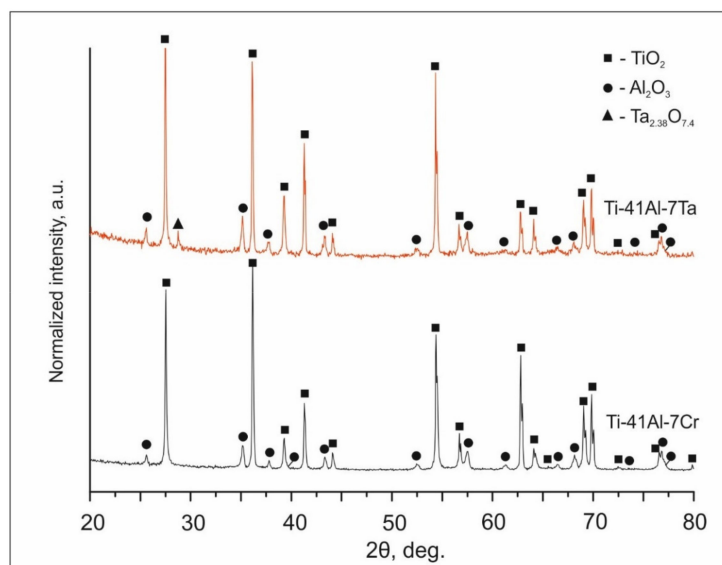


Figure 10. Results of XRD analysis of an oxide scale formed after oxidation at 800 °C for 200 h.

Analysis of the sample surface after oxidation revealed an uneven distribution of the oxide film (Figure 9b,c). Along with the areas characterized by a developed surface (Figure 9b), zones with a thin oxide layer and signs of delamination were observed (Figure 9c). To determine the oxide layer composition in different areas, surface mapping was carried out using an EDX analyzer (Figure 11). It was found that the bulky appearing layer consisted mainly of titania (Figure 11b). Mapping of flat areas (Figure 11a) revealed zones enriched with aluminum, chromium, and oxygen. Titanium-enriched areas were depleted in oxygen. The latter probably corresponded to the initial alloy and areas with a light contrast in Figures 9c and 11 contained aluminum oxide. It suggests that the oxide layer has peeled off, exposing the surface of the test specimen.

It should be noted that the areas containing alumina were enriched in chromium, while the regions with TiO_2 were depleted in chromium. Also, the amount of chromium in the Al_2O_3 zones exceeded that in the bare areas. Since no signs of chromium oxide formation were detected by the XRD analysis (Figure 10), this suggests that the areas where the Al_2O_3 film was formed were initially enriched in chromium, which promotes the formation of alumina. XRD analysis of the oxide layer developed on the surface of the Ti-41Al-7Ta cladding layer revealed that in addition to TiO_2 and Al_2O_3 , tantalum oxide was formed (Figure 10). This phase belongs to metastable tantalum oxides. It is known that equilibrium tantalum oxide is monoclinic Ta_2O_5 . However, besides the stable one, many metastable states of tantalum oxide can exist in a wide range of oxygen concentrations [51]. The obtained tantalum oxide with an approximate stoichiometry of $\text{Ta}_{2.38}\text{O}_{7.4}$ has a hexagonal lattice and belongs to the $P6/mmm$ space group. In the literature, it is referred to as the δ -phase [52].

There are a few studies on the oxidation of an alloy with a composition close to Ti-41Al-7Ta. Hashimoto et al. considered the compositions with up to 5.8 at.% Ta [53]. After 100 h of oxidation at 900 °C, they found a complex oxide layer containing AlTaO_4 and AlTiTaO_6 apart from TiO_2 and Al_2O_3 . Mitoraj and Godlewska [54] found Ta dissolved in titania, substituting the Ti atoms when Ti-46Al-8Ta alloy was exposed to cyclic oxidation at 800 °C. In the hot corrosion conditions at different environments, at the surface of such an alloy, ϵ - Ta_2O_5 was found to be formed by Godlewska et al. in [55]. Thus, the data on the oxide layer composition forming on the surface of Ti-Al-Ta alloys and its effect on their oxidation properties are still quite contradictory and require further research. At the same time, it was mentioned in a number of studies that the oxidation resistance increase upon the addition of tantalum to titanium-based alloys, including TiAl-based alloys, is rather caused not by the composition of the oxide film formed on their surface but by

the formation of an intermediate Ta-enriched layer between the alloy and the oxide film, which suppresses diffusion [53], and by a decrease in solubility of oxygen in the base alloy induced by Ta [56]. It was also mentioned in [56] that Ta is able to decrease the mobility of titanium atoms in binary Ti-Ta alloys, which leads to a decrease in the growth rate of the TiO_2 oxide film.

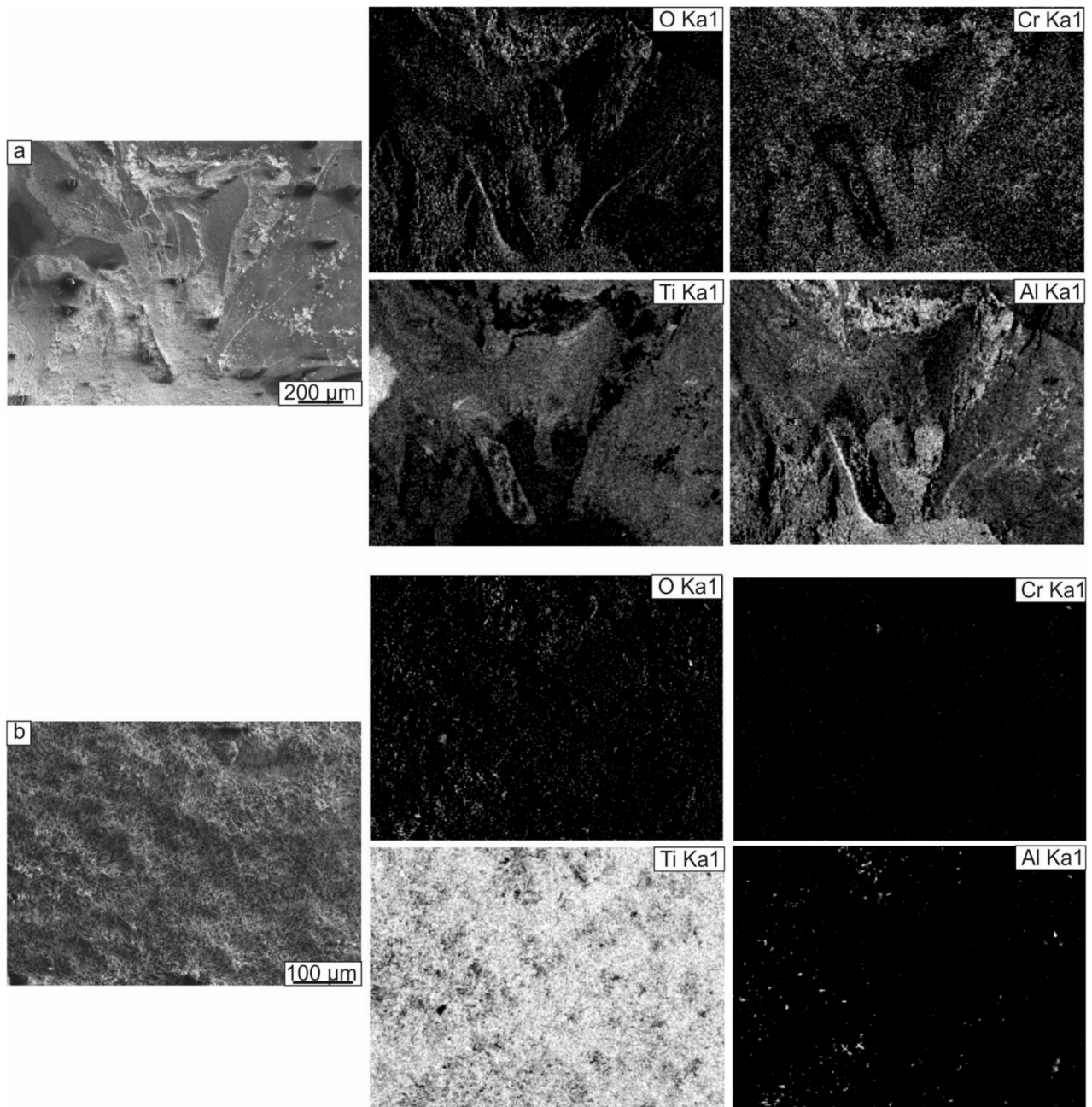


Figure 11. Oxide scale formed after oxidation at 800 °C for 200 h on a surface of Ti-41Al-7Cr alloy: (a) Al_2O_3 region, (b) TiO_2 region. Results of EDX analysis.

SEM analysis of the Ti-41Al-7Ta sample surface after oxidation (Figure 9d) revealed that the surface of the oxide film was less developed than that found at the Ti-41Al-7Cr sample. Some zones were characterized by delamination of the oxide film so that the original composition of the alloy was detected on the surface (Figure 12). It is evidenced by the inhomogeneous distribution of oxygen and titanium over the surface. The brighter contrast in Figure 12 corresponded to the oxidized areas. The elemental distribution gives a reason to believe that the layer contained a mixture of various oxides.

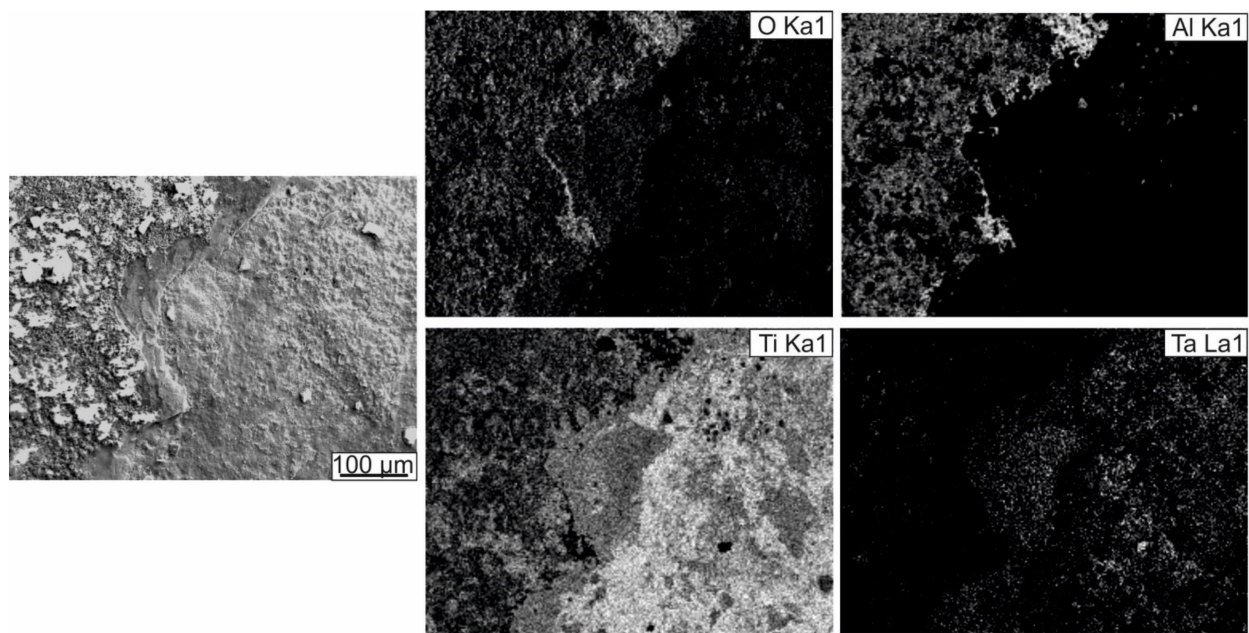


Figure 12. Oxide scale formed after oxidation at 800 °C for 200 h on a surface of Ti-41Al-7Ta alloy. Results of EDX analysis.

4. Discussion

Being β -stabilizing elements for titanium, Ta and Cr nevertheless have a slightly different effect on the structure and properties of TiAl-based alloys when added to the cladding layer. First, this concerns the features of phase formation in alloys. With an actual content of ~41 at.% Al and ~7 at.% of the alloying element, the appearance of α_2 , γ , and β /B2 phases was expected in both alloys. In fact, these phases were found in the cladding layers; however, the ω' phase was additionally formed in the alloy with tantalum.

The issues concerning the formation of ω -related phases in TiAl-based alloys with β -stabilizers are widely discussed in the literature. Precipitations of ω -related phases in the β /B2 matrix were found in alloys with additions of niobium [29,32,33,57], in the 4Zr-4Nb alloy [58], in alloys with Mo [59], V [60], Cr [61], etc. Shao and Tsakirooulos [62] analyzed the stability of ω phase in Ti-Al-X alloys as a function of the aluminum content and the type of transition element added to the alloy. They supposed that deviation of the ω structure from the ideal crystalline lattice of B2 (Δ) and electron concentration in β /B2 phase lattice are the main parameters that influence the stability of the ω phase. With an increase in the concentration of valence electrons in the β /B2 phase, the stability of the ω phase decreases. It means that an increase in the content of aluminum with a low concentration of valence electrons leads to a decrease in the overall electron concentration, which increases the stability of the ω phase. According to [62], the ω phase is unlikely to form in alloys with a parameter ϕ (the free electron per atom per volume of the β unit cell) of more than 0.135 and a large value of Δ . According to their data, the β phase in the Ti-Al-Cr alloys meets these conditions. At the same time, studying Ti-Al-Cr alloys of various compositions, Shao and Tsakirooulos [61] found that ω phase can be stabilized at certain concentrations of chromium and aluminum, and analyzed the stability of the ω phase depending on the chromium content. They found that with an increase in Cr concentration, the ω phase stability decreased. According to the XRD data obtained in our study, the B2 phase in the cladding layer obtained in our study is depleted in aluminum and enriched in chromium, suggesting that the conditions necessary for the formation of the ω phase were not achieved.

Since the value of ϕ also includes the volume of the unit cell, it is reasonable to assume that the atomic radius of the alloying element also plays a role in addition to the electron concentration factor. The atomic radius of chromium is smaller than that of Ta (128 pm vs. 220 pm). It means that under otherwise identical conditions, the cell volume of

the B2 phase containing tantalum should be larger compared to that of the B2 phase alloyed with chromium, and the value of ϕ should be lower. In other words, the stability of the ω phase should increase with the replacement of chromium with tantalum. This assumption is confirmed by the data of [63], where abnormal stability of the ω phase was observed for the Ti-44Al-4Zr-4Ta-0.2Si alloy. Shao and Tsakiroopoulos [61] associated this phenomenon with the size factor. Indeed, atomic radii of both Ta and Zr are higher than that of Cr.

Another essential difference between Ti-41Al-7Ta and Ti-41Al-7Cr cladding layers is the different fractions of the formed phases. From XRD data, it follows that the B2 phase volume fraction in the cladding layer alloyed with chromium was significantly higher than in the tantalum-containing layer (26.5 vol.% vs. 4.8 vol.% (B2 + ω) respectively). According to [64], different elements have a different stabilizing effect on titanium alloys, which can be estimated using the molybdenum equivalent (Mo Eq). The β -stabilizing effect of the elements is evaluated relative to molybdenum, which is taken to be one. The higher the Mo Eq, the higher the β -phase stabilization effect of the component. Thus, the Cr stabilization factor equals 1.6, while that of Ta is 0.22. Consequently, chromium is a stronger β -stabilizer for titanium than tantalum. On the contrary, aluminum is an α -stabilizer and contributes to the increase of the $\alpha \rightarrow \beta$ transformation temperature. Considering that the aluminum concentration in both cladding layers was approximately the same, the main contribution to the stabilization of the β /B2 phase was made by the alloying element. The difference in the fraction of phases in Ti-41Al-7Cr and Ti-41Al-7Ta alloys directly affected the wear and oxidation resistance of the cladding layers.

It is known that the wear resistance of titanium aluminides depends on a number of factors, namely phase composition, presence of hard precipitations, microstructural features, crystalline size, etc. [17]. Wear resistance also significantly depends on the physical and mechanical properties of the separate phases, such as hardness, elastic modulus, and yield strength. Thus, according to [65], there is an inverse linear relationship between hardness and abrasive wear rate: with increasing hardness, the intensity of wear decreases. In the case of multi-phase materials, the hardness of each component as well as their proportion in the material structure will contribute to the average hardness. Okada et al. [28] used the nanoindentation method to measure the hardness of separate phases in the $\gamma + \beta$ alloy of the Ti-44Al-4Cr composition. This method is quite reliable for determining the properties of a specific phase since it excludes the influence of additional factors, such as e.g., grain size. The authors have shown that the hardness of the intermetallic phases did not depend on the content of the alloying elements in them and was equal to 3.1 GPa and 6.9 GPa for the γ and β phases, respectively. In [66], the microhardness values measured for the γ phase were essentially different and varied in the range between 5.2 and 6.8 GPa. The nanohardness of the α_2 phase was higher and reached values ranging from 7.4 to 9.3 GPa. Slightly different values were also obtained by Wang et al. [67], but nevertheless, the hardness ratio of γ to α_2 phases was approximately the same. Thus, in a first approximation, one can conclude that the presence of the γ phase commonly reduces the hardness of the alloy. According to the results of X-ray diffraction analysis, the γ phase fraction in the cladding layer alloyed with tantalum was higher than in the chromium-containing alloy. In addition, the content of β /B2 phase characterized by higher hardness, compared to γ phase, in the tantalum-containing alloy was lower.

At the same time, the tantalum-alloyed layer showed the best resistance to oxidation, which may be due to several reasons. First, this can also be associated with differences in the phase fractions forming the microstructure of the alloys. Different phases exhibit different oxidation resistance. Among γ and α_2 phases, the γ phase is more oxidation resistant [3]. With a decrease of its fraction in the alloy, the oxidation rate increases. At the same time, it is known that the diffusion coefficient of oxygen at 800 °C is significantly higher for the B2 phase compared to α_2 -Ti₃Al, and interaction of B2 with oxygen leads to the predominant TiO₂ formation [68]. Thus, the chromium-containing alloy with a higher B2 fraction and lower amount of γ phase oxidized more rapidly than the Ti-41Al-7Ta alloy. In addition, such factors as forming a Ta-O-based oxide film could influence the oxidation

rate; however, its contribution to oxidation resistance is difficult to estimate based on the available data.

In addition, it should be noticed that the cladding layers were oxidation tested with the substrate removed. If applied to a substrate, as would be the situation in service, one can expect a higher oxidation resistance compared to the value obtained by testing. The reason for that is the inhomogeneous distribution of alloying elements in the depth of the layer. According to EDX analysis, Al and Ta/Cr concentrations were higher in the surface part of the intermetallic layers. It means that the outer surface of intermetallic layers should provide even better oxidation resistance than that obtained in the tests.

Summarizing the data obtained, one can conclude that the choice of an alloying element for TiAl-based alloys used for cladding of pure titanium depends on the expected operating conditions. To increase the wear resistance of the TiAl-based cladding layer, it is necessary to add elements that increase the proportion of hard phases in the coating structure. For this reason, it also seems to be rational to add carbon and boron, which can generate hard particles in the structure. Cladding layers for high-temperature application should be alloyed with an element capable of limiting the mobility of titanium atoms and ensuring the formation of phases prone to form a protective Al_2O_3 layer upon interaction with oxygen.

5. Conclusions

1. The non-vacuum electron-beam cladding of Ti-Al-Ta and Ti-Al-Cr powder mixtures was used to form protective intermetallic layers with a thickness of up to 2 mm on pure titanium substrates. The cladding layers were defect-free and did not contain cracks or visible voids.
2. Providing the same atomic concentrations of Ta and Cr in the initial powder mixtures, cladding layers with different phase compositions and different fractions of phases were formed. In the Ti-41Al-7Cr cladding layer, α_2 , γ , and B2 phases were observed. In addition to the phases mentioned above, the ω' phase was formed in the layer alloyed with tantalum. The volume fractions of α_2 , γ , and B2/ ω' phases in the cladding layers depended on the β -stabilizing effect of the alloying element. Being a stronger β -stabilizer, Cr promoted a larger amount of B2 phase in the structure of the cladding layer compared to tantalum (26 vol.% vs. 4.8 vol.%, respectively).
3. Wear resistance of intermetallic layers depended on the proportion of hard phases in their structure and, consequently, on the type of element that stabilizes certain phases. At abrasive friction, the best results were obtained for the chromium-containing cladding layer characterized by a lower fraction of the soft γ -phase. However, the tantalum-containing cladding layer has also improved the wear resistance of pure titanium. The relative wear resistance of the Ti-41Al-7Ta and Ti-41Al-7Cr was 1.6 and 2.1 times higher than that of pure titanium.
4. The resistance to oxidation of the cladding layers was determined by the types of phases formed and their fraction and the type of alloying element, and its ability to promote an Al_2O_3 oxide film formation. Alloying the intermetallic compound with tantalum and chromium contributed to forming a mixed oxide scale on the surfaces of the samples heated at 800 °C for 200 h. However, on the surface of the Ti-41Al-7Cr sample, large areas consisting only of TiO_2 were formed. The Ti-41Al-7Ta cladding layer exhibited the best protective properties under high-temperature exposure. Its oxidation resistance was 8 times higher compared to the substrate material.
5. From the comparison of the layers alloyed with Ta and Cr, it follows that the choice of alloying element depends on the operation condition. While Ta provides better heat resistance, cladding layers alloyed with Cr possess higher wear properties. At the same time, the difference in Ta- and Cr-containing cladding layer properties was not significant. Considering the high price of Ta, the choice of Cr as an alloying element seems to be more rational.

Author Contributions: Conceptualization, D.V.L.; methodology, M.G.G.; validation, I.Y.P. and A.A.R.; formal analysis, D.V.L. and I.S.L.; investigation, D.V.L., I.Y.P. and A.S.; resources, M.G.G. and F.P.; data curation, I.A.B. and I.Y.P.; writing—original draft preparation, D.V.L.; writing—review and editing, I.A.B. and F.P.; visualization, A.A.R.; supervision F.P.; project administration, D.V.L.; funding acquisition, I.A.B. All authors have read and agreed to the published version of the manuscript.

Funding: This study was funded according to the Federal Task of Ministry of Education and Science of the Russian Federation (project FSUN-2020-0014 (2019-0931): “Investigations of Metastable Structures Formed on Material Surfaces and Interfaces under Extreme External Impacts”). Structural research was conducted at NSTU Materials Research Center.

Data Availability Statement: The data presented in this study are available on request from the corresponding author.

Conflicts of Interest: The authors declare no conflict of interest.

References

- Bansal, R.; Singh, J.K.; Singh, V.; Singh, D.D.N.; Das, P. Optimization of Oxidation Temperature for Commercially Pure Titanium to Achieve Improved Corrosion Resistance. *J. Mater. Eng. Perform.* **2017**, *26*, 969–977. [\[CrossRef\]](#)
- Jamesh, M.; Sankara Narayanan, T.S.N.; Chu, P.K. Thermal Oxidation of Titanium: Evaluation of Corrosion Resistance as a Function of Cooling Rate. *Mater. Chem. Phys.* **2013**, *138*, 565–572. [\[CrossRef\]](#)
- Leyens, C.; Perters, M. (Eds.) *Titanium and Titanium Alloys: Fundamentals and Application*; Wiley-VCH: Weinheim, Germany, 2003.
- Lütjering, G.; Williams, J.C. *Titanium*; Derby, B., Ed.; Springer: Berlin/Heidelberg, Germany; New York, NY, USA, 2007; p. 442.
- Chechulin, B.B.; Ushakov, S.S.; Razuvaeva, I.N.; Goldfain, V.N. *Titanovoye Splavy V Mashinostroenii*; Mashinostroenie: Leningrad, Russia, 1977; p. 248.
- Smialek, J.L. Oxidation Behaviour of TiAl₃ Coatings and Alloys. *Corros. Sci.* **1993**, *35*, 1199–1208. [\[CrossRef\]](#)
- Zhang, Z.G.; Peng, Y.P.; Mao, Y.L.; Pang, C.J.; Lu, L.Y. Effect of Hot-Dip Aluminizing on the Oxidation Resistance of Ti-6Al-4V Alloy at High Temperatures. *Corros. Sci.* **2012**, *55*, 187–193. [\[CrossRef\]](#)
- Zhang, Z.G.; Peng, Y.P.; Mao, Y.L.; Hou, C.M.; Xu, L. Hot-Dip Aluminizing Fabrication of TiAl₃ Coating on TA15 Alloy and Its High Temperature Oxidation Behaviors. *High Temp. Mater. Process.* **2012**, *30*, 519–525.
- Leyens, C.; Peters, M.; Kaysser, W.A. Intermetallic Ti-Al Coatings for Protection of Titanium Alloys: Oxidation and Mechanical Behavior. *Surf. Coat. Technol.* **1997**, *94*, 34–40. [\[CrossRef\]](#)
- Guo, C.; Zhou, J.; Zhao, J.; Wang, L.; Yu, Y.; Chen, J.; Zhou, H. Improvement of the Oxidation and Wear Resistance of Pure Ti by Laser-Cladding Ti₃Al Coating at Elevated Temperature. *Tribol. Lett.* **2011**, *42*, 151–159. [\[CrossRef\]](#)
- Zhang, Y.; Li, H.; Zhang, K. Investigation of the Laser Melting Deposited TiAl Intermetallic Alloy on Titanium Alloy. *Adv. Mater. Res.* **2011**, *146*, 1638–1641. [\[CrossRef\]](#)
- Guo, B.; Zhou, J.; Zhang, S.; Zhou, H.; Pu, Y.; Chen, J. Phase Composition and Tribological Properties of Ti-Al Coatings Produced on Pure Ti by Laser Cladding. *Appl. Surf. Sci.* **2007**, *253*, 9301–9310. [\[CrossRef\]](#)
- Guo, B.; Zhou, J.; Zhang, S.; Zhou, H.; Pu, Y.; Chen, J. Tribological Properties of Titanium Aluminides Coatings Produced on Pure Ti by Laser Surface Alloying. *Surf. Coat. Technol.* **2008**, *202*, 4121–4129. [\[CrossRef\]](#)
- Mizuta, N.; Matsuura, K.; Kirihara, S.; Miyamoto, Y. Titanium Aluminide Coating on Titanium Surface Using Three-Dimensional Microwelder. *Mat. Sci. Eng. A* **2008**, *492*, 199–204. [\[CrossRef\]](#)
- Matsubara, T.; Shibutani, T.; Uenishi, K.; Kobayashi, K.F. Fabrication of a Thick Surface Layer of Al₃Ti on Ti Substrate by Reactive-Pulsed Electric Current Sintering. *Intermetallics* **2000**, *8*, 815–822. [\[CrossRef\]](#)
- Lazurenko, D.V.; Bataev, I.A.; Laptev, I.S.; Ruktuev, A.A.; Maliutina, I.N.; Golkovsky, M.G.; Bataev, A.A. Formation of Ti-Al Intermetallics on a Surface of Titanium by Non-Vacuum Electron Beam Treatment. *Mater. Charact.* **2017**, *134*, 202–212. [\[CrossRef\]](#)
- Appel, F.; Paul, J.D.H.; Oehring, M. *Gamma Titanium Aluminide Alloys*; Wiley-VCH: Weinheim, Germany; GmbH&Co. KGaA: Weinheim, Germany, 2011; p. 752.
- Huang, S.-C.; Hall, E.L. Effects of Cr Additions to Binary TiAl-Base Alloys. *Metall. Trans. A* **1991**, *22*, 2619–2627. [\[CrossRef\]](#)
- Clemens, H.; Wallgram, W.; Kremmer, S.; Güther, V.; Otto, A.; Bartels, A. Design of Novel β -Solidifying TiAl Alloys with Adjustable β /B2-Phase Fraction and Excellent Hot-Workability. *Adv. Eng. Mater.* **2008**, *10*, 707–713. [\[CrossRef\]](#)
- Wu, X. Review of Alloy and Process Development of TiAl Alloys. *Intermetallics* **2006**, *14*, 1114–1122. [\[CrossRef\]](#)
- Vojtěch, D.; Popela, T.; Hamáček, J.; Kützendörfer, J. The Influence of Tantalum on the High Temperature Characteristics of Lamellar Gamma+Alpha₂ Titanium Aluminide. *Mater. Sci. Eng. A* **2011**, *528*, 8557–8564. [\[CrossRef\]](#)
- Appel, F.; Brossmann, U.; Christoph, U.; Eggert, S.; Janschek, P.; Lorenz, U. Recent Progress in the Development of Gamma titanium Aluminide Alloys. *Adv. Eng. Mater.* **2000**, *2*, 699–720. [\[CrossRef\]](#)
- Wang, J.N.; Wang, Y. An Investigation of the Origin of the Superplasticity of Cast TiAl Alloys. *Int. J. Plast.* **2006**, *22*, 1530–1548. [\[CrossRef\]](#)

24. Lazurenko, D.V.; Laptev, I.S.; Golkovsky, M.G.; Stark, A.; Paul, J.; Bataev, I.; Ruktuev, A.A.; Song, L.; Gollwitzer, C.; Pyczak, F. Influence of the Ti/Al/Nb Ratio on the Structure and Properties on Intermetallic Layers Obtained on Titanium by Non-vacuum Electron Beam Cladding. *Mater. Charact.* **2020**, *163*, 110246. [[CrossRef](#)]
25. Lutterotti, L.; Matthies, S.; Wenk, H.-R. MAUD: A Friendly Java Program for Material Analysis Using Diffraction. In Proceedings of the IUCr: Newsletter of the CPD, McGill University, Montreal, QC, Canada, 9–13 August 1999; pp. 14–15.
26. Scientific Group Thermodata Europe. *Binary Systems. Part 1 _ Elements and Binary Systems from Ag-Al to Au-Tl Al-Mn: Datasheet from Landolt-Börnstein-Group IV Physical Chemistry Volume 19B1: "Binary Systems. Part 1 _ Elements and Binary Systems from Ag-Al to Au-Tl" in SpringerMaterials (10.1007/10655491_41)*; Springer: Berlin/Heidelberg, Germany, 2002.
27. Sauthoff, G. *Intermetallics*; Wiley: Hoboken, NJ, USA, 2008.
28. Okada, Y.; Taniguchi, S.; Yamagata, R.; Nakashima, H.; Takeyama, M. Nano-Indentation Modulus and Hardness of β -Ti and γ -TiAl Phases in Ti–Al–Cr System. *MRS Adv.* **2021**, *6*, 183–186. [[CrossRef](#)]
29. Bendersky, L.A.; Boettinger, W.J.; Burton, B.P.; Biancianiello, F.S.; Shoemaker, C.B. The Formation of Ordered ω -Related Phases in Alloys of Composition Ti₄Al₃Nb. *Acta Metall. Et Mater.* **1990**, *38*, 931–943. [[CrossRef](#)]
30. Stark, A.; Oehring, M.; Pyczak, F.; Schreyer, A. In Situ Observation of Various Phase Transformation Paths in Nb-Rich TiAl Alloys during Quenching with Different Rates. *Adv. Eng. Mater.* **2011**, *13*, 700–704. [[CrossRef](#)]
31. Zhu, B.; Xue, X.; Kou, H.; Li, X.; Li, J. Effect of Microstructure on the Fracture Toughness of Multi-Phase High Nb-Containing TiAl Alloys. *Intermetallics* **2018**, *100*, 142–150. [[CrossRef](#)]
32. Stark, A.; Bartels, A.; Clemens, H.; Schimansky, F.P. On the Formation of Ordered ω -phase in High Nb Containing γ -TiAl Based Alloys. *Adv. Eng. Mater.* **2008**, *10*, 929–934. [[CrossRef](#)]
33. Song, L.; Zhang, L.Q.; Xu, X.J.; Sun, J.; Lin, J.P. Omega Phase in As-Cast High-Nb-Containing TiAl Alloy. *Scr. Mater.* **2013**, *68*, 929–932. [[CrossRef](#)]
34. Jewett, T.J.; Ahrens, B.; Dahms, M. Stability of TiAl in the Ti–Al–Cr System. *Mat. Sci. Eng. A* **1997**, *225*, 29–37. [[CrossRef](#)]
35. Chen, H.; Weitzer, F.; Krendelsberger, N.; Du, Y.; Schuster, J.C. Reaction Scheme and Liquidus Surface of the Ternary System Aluminum–Chromium–Titanium. *Metall. Mater. Trans. A* **2009**, *40*, 2980. [[CrossRef](#)]
36. Ye, L.-H.; Wang, H.; Zhou, G.; Hu, Q.-M.; Yang, R. Phase Stability of TiAl-X (X=V, Nb, Ta, Cr, Mo, W, and Mn) Alloys. *J. Alloys Compd.* **2020**, *819*, 153291. [[CrossRef](#)]
37. Strychor, R.; Williams, J.C.; Soffa, W.A. Phase Transformations and Modulated Microstructures in Ti–Al–Nb Alloys. *Metall. Trans. A* **1988**, *19*, 225–234. [[CrossRef](#)]
38. Hsiung, L.M.; Cai, W.; Wadley, H.N.G. Microstructure and Phase Evolution in Rapidly-Solidified Ti–24Al–11Nb. In *High Temperature Aluminides and Intermetallics*; Whang, S.H., Pope, D.P., Liu, C.T., Eds.; Elsevier: Oxford, UK, 1992; pp. 295–303.
39. Han, T.; Huang, Z.W. Microstructures and Tensile Properties of Ti-46Al-8Ta after Heat Treatment and Thermal Exposure. *Cailiao Kexue Yu Gongyi Mater. Sci. Technol.* **2013**, *21*, 90–95.
40. Buenconsejo, P.J.S.; Kim, H.Y.; Hosoda, H.; Miyazaki, S. Shape Memory Behavior of Ti-Ta and Its Potential as a High-temperature Shape Memory Alloy. *Acta Mater.* **2009**, *57*, 1068–1077. [[CrossRef](#)]
41. Ferrari, A.; Paulsen, A.; Frenzel, J.; Rogal, J.; Eggeler, G.; Drautz, R. Unusual Composition Dependence of Transformation Temperatures in Ti-Ta-X Shape Memory Alloys. *Phys. Rev. Mater.* **2018**, *2*, 073609. [[CrossRef](#)]
42. Niendorf, T.; Krooß, P.; Batyrsina, E.; Paulsen, A.; Motemani, Y.; Ludwig, A.; Buenconsejo, P.; Frenzel, J.; Eggeler, G.; Maier, H.J. Functional and Structural Fatigue of Titanium Tantalum High Temperature Shape Memory Alloys (HT SMAs). *Mater. Sci. Eng. A* **2015**, *620*, 359–366. [[CrossRef](#)]
43. Imayev, V.; Khismatullin, T.; Oleneva, T.; Imayev, R.; Valiev, R.; Wunderlich, R.; Minkow, A.; Hecht, U.; Fecht, H.J. Grain Refinement in Cast Ti-46Al-8Nb AND Ti-46Al-8Ta Alloys Via Massive Transformation. *Adv. Eng. Mater.* **2008**, *10*, 1095–1100. [[CrossRef](#)]
44. Xu, X.-J.; Song, L.; Jin, X.-O.; Han, D.-D.; Wang, X.; Lin, J.-P. Microstructure and Microsegregation of Directionally Solidified Ti–45Al–8Nb Alloy with Different Solidification Rates. *Rare Met.* **2016**, *35*, 70–76. [[CrossRef](#)]
45. Khanna, A.S. Chapter 6-High-Temperature Oxidation. In *Handbook of Environmental Degradation of Materials*, 3rd ed.; Kutz, M., Ed.; William Andrew Publishing: Norwich, NY, USA, 2018; pp. 117–132.
46. Dai, J.; Zhu, J.; Chen, C.; Weng, F. High Temperature Oxidation Behavior and Research Status of Modifications on Improving High Temperature Oxidation Resistance of Titanium Alloys and Titanium Aluminides: A Review. *J. Alloys Compd.* **2016**, *685*, 784–798. [[CrossRef](#)]
47. Zhou, C.; Yang, Y.; Gong, S.; Xu, H. Effect of Ti–Al–Cr Coatings on the High Temperature Oxidation Behavior of TiAl Alloys. *Mater. Sci. Eng. A* **2001**, *307*, 182–187. [[CrossRef](#)]
48. Laska, N.; Braun, R.; Knittel, S. Oxidation Behavior of Protective Ti–Al–Cr Based Coatings Applied on the γ -TiAl Alloys Ti-48-2-2 and TNM-B1. *Surf. Coat. Technol.* **2018**, *349*, 347–356. [[CrossRef](#)]
49. Jacobson, N.S.; Brady, M.P.; Mehrotra, G.M. Thermodynamics of Selected Ti–Al and Ti–Al–Cr alloys. *Oxid. Met.* **1999**, *52*, 537–556. [[CrossRef](#)]
50. Brady, M.P.; Smialek, J.L.; Smith, J.; Humphrey, D.L. The Role of Cr in Promoting Protective Alumina Scale Formation by γ -Based Ti–Al–Cr alloys—I. Compatibility with Alumina and Oxidation Behavior in Oxygen. *Acta Mater.* **1997**, *45*, 2357–2369. [[CrossRef](#)]
51. Wasilewski, R.J. The Solubility of Oxygen in, and the Oxides of, Tantalum. *J. Am. Chem. Soc.* **1953**, *75*, 1001–1002. [[CrossRef](#)]

52. Donaldson, O.K.; Hattar, K.; Trelewicz, J.R. Metastable Tantalum Oxide Formation during the Devitrification of Amorphous Tantalum Thin Films. *J. Am. Ceram. Soc.* **2016**, *99*, 3775–3783. [[CrossRef](#)]
53. Hashimoto, K.; Seita, K. Formation of Protective Intermediate Phase in Ta Addition TiAl during High Temperature Oxidation. *Mater. Sci. Forum* **2010**, *654-656*, 546–549. [[CrossRef](#)]
54. Mitoraj, M.; Godlewska, E.M. Oxidation of Ti-46Al-8Ta in air at 700 °C and 800 °C under Thermal Cycling Conditions. *Intermetallics* **2013**, *34*, 112–121. [[CrossRef](#)]
55. Godlewska, E.; Mitoraj, M.; Leszczynska, K. Hot Corrosion of Ti-46Al-8Ta (at.%) Intermetallic Alloy. *Corros. Sci.* **2014**, *78*, 63–70. [[CrossRef](#)]
56. Hanrahan, R.J.; Butt, D.P. Oxidation Kinetics and Mechanisms of Ti-Ta Alloys. *Oxid. Met.* **1997**, *47*, 317–353. [[CrossRef](#)]
57. Huang, Z.W.; Voice, W.; Bowen, P. Thermal Exposure Induced $\alpha_2 + \gamma \rightarrow \beta_2(\omega)$ and $\alpha_2 \rightarrow \beta_2(\omega)$ Phase Transformations in a High Nb fully Lamellar TiAl Alloy. *Scr. Mater.* **2003**, *48*, 79–84. [[CrossRef](#)]
58. Huang, Z.W. Ordered ω Phases in a 4Zr-4Nb-Containing TiAl-Based Alloy. *Acta Mater.* **2008**, *56*, 1689–1700. [[CrossRef](#)]
59. Morris, M.A.; Li, Y.G. Deformation Mechanisms and Slip Transfer in a Ti44Al2Mo Alloy. *Mat. Sci. Eng. A* **1995**, *197*, 133–145. [[CrossRef](#)]
60. Shao, G.; Miodownik, A.P.; Tsakirooulos, P. ω -Phase Formation in V-Al and Ti-Al-V Alloys. *Philos. Mag. A Phys. Condens. Matter Struct. Defects Mech. Prop.* **1995**, *71*, 1389–1408. [[CrossRef](#)]
61. Shao, G.; Tsakirooulos, P. On the ω Phase Formation in Cr-Al and Ti-Al-Cr Alloys. *Acta Mater.* **2000**, *48*, 3671–3685. [[CrossRef](#)]
62. Shao, G.; Tsakirooulos, P. Prediction of ω Phase Formation in Ti-Al-X alloys. *Mater. Sci. Eng. A* **2002**, *329-331*, 914–919. [[CrossRef](#)]
63. Cheng, T.T.; Loretto, M.H. Preliminary Study on the Decomposition of the Beta Phase in Ti-44Al-8Nb and Ti-44Al-4Ta-4Zr-0.2Si. In *Structural Intermetallics*; Nathal, M.V., Ed.; Minerals, Metals and Materials Society: Warrendale, PA, USA, 1997; pp. 253–260.
64. Weiss, I.; Semiatin, S.L. Thermomechanical Processing of Beta Titanium Alloys—An Overview. *Mater. Sci. Eng. A* **1998**, *243*, 46–65. [[CrossRef](#)]
65. Blau, P.J. *Friction, Lubrication, and Wear Technology*, 18th ed.; Harvard: Cambridge, MA, USA, 1992; Volume 18.
66. Göken, M.; Kempf, M.; Nix, W.D. Hardness and Modulus of the lamellar Microstructure in PST-TiAl Studied by Nanoindentations and AFM. *Acta Mater.* **2001**, *49*, 903–911. [[CrossRef](#)]
67. Wang, D.P.; Qi, Z.X.; Zhang, H.T.; Chen, G.; Lu, Y.; Sun, B.A.; Liu, C.T. Microscale Mechanical Properties of Ultra-High-Strength Polysynthetic TiAl-Ti3Al Single Crystals. *Mater. Sci. Eng. A* **2018**, *732*, 14–20. [[CrossRef](#)]
68. Chen, J.; Chen, Q.; Qu, S.J.; Xiang, H.P.; Wang, C.; Gao, J.B.; Feng, A.H.; Chen, D.L. Oxidation Mechanisms of an Intermetallic Alloy at High Temperatures. *Scr. Mater.* **2021**, *199*, 113852. [[CrossRef](#)]